Nanocap-Shaped Tin Phthalocyanines: Synthesis, Characterization, and Corrosion Inhibition Activity

Hiram I. Beltrán,*[a] Raquel Esquivel,[a] Marcelo Lozada-Cassou,[a] Marco A. Dominguez-Aguilar,[a] Arturo Sosa-Sánchez,[b] Jose L. Sosa-Sánchez,*[b] Herbert Höpfl,[c] Victor Barba,[c] Rolando Luna-García,[c] Norberto Farfán,[d] and Luis S. Zamudio-Rivera*[a]

Abstract: Thermal and microwave reactions between [$PcSn^{IV}Cl_2$] (**1**) and the potassium salts of eight fatty acids (**2a–h**) led to *cis*-[$(RCO_2)_2Sn^{IV}Pc$] compounds (**3a–h**) in yields ranging from 54 to 90%. Compounds **3a–h** were fully characterized by elemental analysis, spectroscopy (IR, UV/Vis, multinuclear NMR), and seven X-ray diffraction structures, whereby two different allotropes were observed in two cases. The two carboxylates in **3** have a *cis* anisobidentate binding mode, octacoordination of the tin atoms with square-antiprismatic geometry, and π-electron-rich nanocap shapes. On account of the latter characteristics, **3a–h** compounds have anticorrosion properties. LPR and Tafel electrochemical methods were used to characterize the behavior of these derivatives in naturally aerated sour brine, which is a common environment in petroleum production and refinery operations. The measurement of the corrosion rate of carbon steel AISI 1018 in the presence of **3a–h** (500 ppm) gave efficiencies of 61–87% for the inhibitor performance. Of the different derivatives examined, compounds **3e** and **3h** were the most effective corrosion inhibitor prototypes.

Keywords: corrosion inhibitor · molecular engineering · phthalocyanines · supramolecular chemistry · tin

Introduction

Phthalocyanine (PcH_2) and its metal complexes (MPcs) were accidentally discovered in the early 1900s.[1] Applications were quickly found for them, and the number of uses have increased considerably since then.[2–11]

The size, charge, and ligand substitution of the metal in MPcs,[11–21] which can be used as a template for the condensation reaction by microwave or thermal irradiation,[22–34] determine the number of oligomeric units, the final conformation of the macrocyclic system, and *cis–trans* isomerism. These factors influence the chemisorption properties with respect to the type of surface (Figure 1).

The discovery of the *cis* configuration and nanocap shape in some axially substituted SnPcs (containing concave, naked, π-electron rich, nanosurfaces) and collateral application of simple MPcs to prevent corrosion[35] prompted our multidisciplinary research efforts[36–41] to test the possibility of using this kind of molecules as corrosion inhibitors.[42–44]

Herein we present two new approaches to *cis*-[bis-(carboxylato)Sn^{IV}] complexes (**3a–h**):[44] 1) thermal synthesis and 2) a microwave (MW) procedure. Complexes **3a–h** were

[a] Dr. H. I. Beltrán, R. Esquivel, Dr. M. Lozada-Cassou, Dr. M. A. Dominguez-Aguilar, Dr. L. S. Zamudio-Rivera
PIM-IMP
Eje Central Lázaro Cárdenas 152, Col. San Bartolo Atepehuacan
C. P. 07730 Mexico D. F. (Mexico)
Fax: (+52) 55-9175-6239
E-mail: hbeltran@imp.mx
lzamudio@imp.mx

[b] A. Sosa-Sánchez, Dr. J. L. Sosa-Sánchez
CIDS-IC-BUAP
Blvd. 14 Sur y Av. San Claudio, Ciudad Universitaria Puebla, Puebla (Mexico)
E-mail: jose.sosa@icbuap.buap.mx.

[c] Dr. H. Höpfl, Dr. V. Barba, R. Luna-García
CIQ-UAEM, Av. Universidad 1001
C. P. 62210 Cuernavaca (Mexico)

[d] Dr. N. Farfán
DQ-CINVESTAV
Apdo. Postal 14—740
C. P. 07000 Mexico D.F. (Mexico)

Supporting information for this article is available on the WWW under http://www.chemeurj.org/ or from the author.

 DOI: 10.1002/chem.200400955

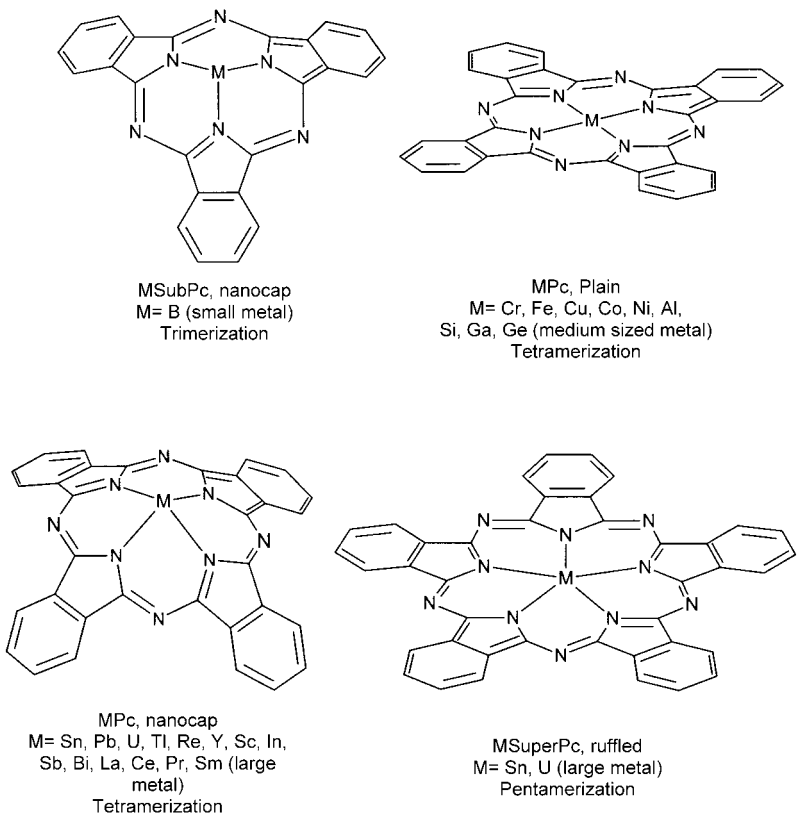

Figure 1. The molecular shape of the Pc ligand in MSubPc, MPc, and MSuperPc.

characterized by elemental analyses, IR, UV/Vis, ^{1}H, ^{13}C, ^{119}Sn NMR spectroscopy and X-ray single-crystal diffraction. Complexes **3a–h** were tested as corrosion inhibitors for steel in sour brine solutions, which simulates a commonly encountered environment in primary plants of the petroleum industry. Preliminary results related to this study have been already published.[44]

Results and Discussion

Thermal and microwave syntheses: In the thermal protocol, $[PcSn^{IV}Cl_2]$[44] (**1**) was allowed to react with the potassium salts of eight fatty acids (**2a–h**) in a 1:2 molar ratio by refluxing the mixtures in DMF for 2.5 h to afford the corresponding *cis*-[bis(carboxylato)Sn^{IV}] complexes (**3a–h**).

Complexes **3a–h** were also obtained by microwave irradiation of the starting materials in DMF for 5 and 10 min. For purposes of comparison, the power was fixed to 300 and 600 W at a setup temperature (ST) of 150 °C (Scheme 1).

When the reaction times were increased, decomposition to 1,2-dicyanobenzene occurred to a greater extent, as demonstrated by ^{1}H and ^{13}C NMR experiments. Compounds **3a–h** were separated from methanol/water solvent mixtures to give pure metallic blue powders in yields ranging from 54 to 78% (thermal procedure) or from 49 to 90% (microwave procedure, Table 1). Both yields are better than those of axial ligand substitution reactions in structurally related MPcs.[4,10,11,16–19,33,39,40,44]

The microwave procedure gave higher yields and required shorter reaction times (by a factor of at least 15) compared to the thermal procedure. Furthermore, the yield improved when the power supply was increased from 300 to 600 W. There were only two cases in which the thermal procedure gave equal or better yields, namely for **3d** and **3f** (see Table 1). The reactions were repeated at least three times to measure the reliability of the results and to unequivocally determine the yields of the two procedures.

Spectroscopic trends: The IR data (see the Experimental Section) provide useful information on the binding mode of

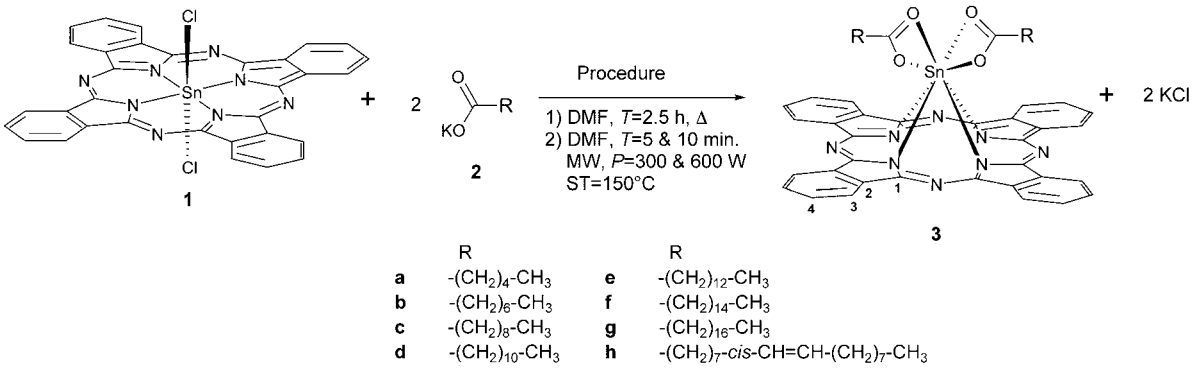

Scheme 1. Thermal and microwave procedures for the preparation of SnPcs **3a–h**.

Table 1. Comparison of yields (%) for the two procedures used for the preparation of **3a–h** compounds.

Compd	Thermal procedure	Microwave procedure			
		300 W		600 W	
	2.5 h	5 min	10 min	5 min	10 min
3a	54	73	80	70	61
3b	55	56	70	80	86
3c	58	69	76	76	74
3d	78	59	49	69	79
3e	63	72	75	83	74
3f	78	60	69	76	73
3g	66	75	77	90	84
3h	62	58	68	82	76

the carboxylate ligands to the tin atoms. In previously reported metalloporphyrin (Mporph) systems with σ-bonded CH_3COO^- fragments (M = Ge and Sn),[45] the ν_{as}(COO) and ν_s(COO) bands appear at 1661–1678 cm^{-1} and at 1269–1294 cm^{-1}, respectively. In contrast, for MPorph systems with isobidentate ligation (M = In and Tl),[45] the ν_{as}(COO) and ν_s(COO) bands appear at 1556–1562 cm^{-1} and 1412–1421 cm^{-1}, respectively. The ν_{as}(COO) and ν_s(COO) bands of compounds **3a–h** were displayed at almost constant values of 1609 cm^{-1} and 1418–1422 cm^{-1}, respectively. This indicates bonding between a sigma (σ) and an isobidentate ligation, which is operative for all the COO^- moieties and is usually referred to as anisobidentate binding.

The signals in the NMR spectra correspond to a quarter of the molecule for the Pc ligand, thus indicating a C_{4v} local symmetry in solution. The hydrocarbon tail signals are related to only half of the molecule owing to a C_{2v} local symmetry.

A summary of the ^{1}H, ^{13}C, and ^{119}Sn NMR data is given in the Supporting Information. The aliphatic ^{1}H signals appear clearly separated on account of the anisotropic effect that influences the -$(CH_2)_n$- protons which are placed within the ring currents of the Pc macrocycle. Thus, five well-separated -CH_2- signals at δ = 0.02–0.52 ppm are shown. A -CH_3 triplet signal is shown at δ = 0.36–1.25 ppm, and the remaining signals overlap within δ = 1.52–1.64 ppm. The signals attributed to α-CH_2 became broader with increasing hydrocarbon tail length, which denotes a fixed orientation of this methylene group as well as an absence of the spin-rotational relaxation mechanism,[44] in addition to information about the anisobidentate coordination character of the $RCOO^-$ group towards the tin atom.

The ^{13}C NMR spectra had to be measured with relaxation times of at least 2.5 s because the signal for the carboxylate group could not be quickly detected at shorter times. This signal appeared at δ = 176.5–177.0 ppm, and that of the quaternary carbon atom at the azo bridge was at δ = 152.6–153.1 ppm, the *ipso*-carbon atom was at δ = 135.6–136.0 ppm, the C_{out} at δ = 129.8–130.4 ppm, and finally the C_{in} at δ = 122.7–123.4 ppm.

The ^{119}Sn chemical shifts have almost constant values of $\delta \approx -846$ ppm,[44] which indicates that no important differences arise with respect to changes in the hydrocarbon tail length.

Table 2. Crystal data and experimental details for **3a**, **3a**·$CHCl_3$, **3b**, **3c-A**, **3c-B**, **3e**, and **3f**.

Compound	**3a**[a]	**3a**·$CHCl_3$[a]	**3b**[a]	**3c-A**[a,c]	**3c-B**[a]	**3e**[b,c]	**3f**[a]
empirical formula	$C_{44}H_{38}N_8O_4Sn$	$C_{44}H_{38}N_8O_4Sn{\cdot}CHCl_3$	$C_{48}H_{46}N_8O_4Sn$	$C_{52}H_{54}N_8O_4Sn$	$C_{52}H_{54}N_8O_4Sn$	$C_{60}H_{70}N_8O_4Sn$	$C_{64}H_{78}N_8O_4Sn$
FW	861.51	980.88	917.62	973.72	973.72	1085.93	1142.03
crystal system	triclinic	triclinic	triclinic	triclinic	triclinic	triclinic	triclinic
space group	$P\bar{1}$	$P\bar{1}$	$P\bar{1}$	$P\bar{1}$	$P\bar{1}$	$P\bar{1}$	$P\bar{1}$
crystal color	metallic blue	metallic blue	metallic blue	metallic blue	metallic blue	metallic blue	metallic blue
cryst. size [mm^3]	0.20×0.28×0.32	0.03×0.03×0.32	0.03×0.01×0.21	0.04×0.31×0.35	0.03×0.2·0×21	0.1×0.1×0.05	0.02×0.21×0.35
a [Å]	12.9079(8)	9.6123(8)	11.7235(11)	13.1764(9)	12.8084(17)	9.559(5)	12.2196(11)
b [Å]	13.1978(8)	14.9210(13)	14.3479(14)	13.4184(9)	12.8325(17)	11.670(5)	13.1624(12)
c [Å]	13.5263(9)	15.6757(13)	14.4524(14)	14.9293(10)	13.9470(19)	25.913(5)	18.0135(16)
α [°]	105.691(1)	69.445(2)	110.877(2)	65.399(1)	87.761(3)	81.983(5)	81.633(2)
β [°]	115.649(1)	78.625(2)	101.076(2)	71.356(1)	85.840(3)	89.708(5)	84.088(2)
γ [°]	102.179(1)	79.257(2)	106.420(2)	78.930(1)	78.093(3)	73.359(5)	85.093(2)
V [$Å^3$]	1851.5(2)	2046.9(3)	2059.2(3)	2268.7(3)	2236.5(5)	2740.7(19)	2843.9(4)
Z	2	2	2	2	2	2	2
ρ_{calcd} [$mg\,m^{-3}$]	1.545	1.591	1.480	1.425	1.446	1.316	1.334
μ [mm^{-1}]	0.748	0.877	0.678	0.620	0.629	0.520	0.505
θ [°]	1.73 to 25.00	1.47 to 25.00	1.60 to 25.00	1.56 to 25.00	1.46 to 25.00	3.20 to 25.39	1.15 to 25.00
coll. refln.	10376	14913	20023	16694	10907	13839	13922
indep. reflns, [R_{int}]	6451 [0.031]	7177 [0.065]	7428 [0.056]	7978 [0.041]	7286 [0.075]	9026 [0.041]	9292 [0.062]
compl. to θ (°) [%]	25.00 [99.0]	25.00 [99.3]	25.00 [99.8]	25.00 [99.7]	25.00 [92.4]	25.34 [89.4]	25.00 [92.6]
data/restr/param	6451/0/516	7177/0/574	7248/7/552	7978/0/588	7287/0/588	9026/0/658	9292/4/696
GOOF	1.066	1.133	1.052	1.037	0.949	1.162	1.070
R_1 [$I > 2\sigma(I)$]	0.0375	0.0745	0.0525	0.0373	0.0726	0.0695	0.0804
R_{2w}(all data)	0.0963	0.1444	0.1235	0.0864	0.1554	0.1580	0.1661
$\Delta\rho_{min}$ [$e\,Å^{-3}$]	−0.914	−1.418	−1.380	−0.671	−1.250	−0.525	−1.466
$\Delta\rho_{max}$ [$e\,Å^{-3}$]	1.529	1.925	1.638	0.926	0.789	0.676	1.115

[a] Data collection on a Bruker-AXS APEX diffractometer. [b] Data collection on an Enraf-Bruker CCD diffractometer. [c] Taken from reference [44] for comparison.

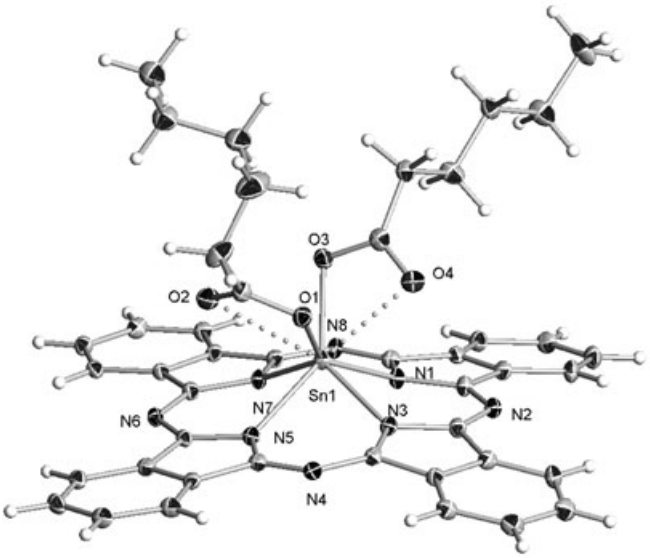

Figure 2. Molecular structure of **3a**.

X-ray diffraction analysis: The crystal data of the starting material used for the reactions outlined in Scheme 1 are summarized in reference [46]; however, this structure has already been described with similar parameters.[47,48] Five of the eight studied compounds were crystallized and most of the relevant crystallographic data is summarized in Table 2 (Figure 2 shows the numbering scheme for **3a**), and the most important geometric variables are reported in Table 3. Interestingly, two polymorphic crystals were obtained for **3a** and **3c**, which thus permitted the analysis of different conformations of the $Sn(OOCR)_2$ backbones.

All compounds crystallized in form of thin overlapping sheets, as shown by SEM micrographs of **3a**·$CHCl_3$, **3b**, and **3c-A** (see the Supporting Information).

In all compounds characterized by X-ray crystallography, the tin atoms have a coordination number of eight with two sets of O–Sn and O···Sn bonds. The interatomic distances range from 2.080 to 2.117 Å and from 2.484 to 2.858 Å, respectively (the van der Waals radius is 1.52 Å and 2.17 Å for

Table 3. Structural details for **3a**, **3a**·$CHCl_3$, **3b**, **3c-A**, **3c-B**, **3e** and **3f**.

Compound	**3a**	**3a**·$CHCl_3$	**3b**	**3c-A**	**3c-B**	**3e**	**3f**
bond lengths [Å]							
Sn–O	2.095(2)	2.082(4)	2.080(3)	2.102(2)	2.100(5)	2.100(4)	2.071(4)
	2.137(2)	2.117(5)	2.092(3)	2.104(2)	2.109(5)	2.101(5)	2.125(4)
Sn···O	2.432(2)	2.543(5)	2.574(3)	2.545(2),	2.522(5)	2.627(6)	2.484(5)
	2.692(2)	2.757(5)	2.830(4)	2.627(2)	2.677(5)	2.691(6)	2.858(5)
Sn–N_i	2.158(3)	2.134(5)	2.166(4)	2.148(2)	2.142(6)	2.143(5)	2.140(5)
	2.162(2)	2.155(5)	2.181(4)	2.158(2)	2.146(6)	2.154(5)	2.161(5)
	2.178(2)	2.161(6)	2.145(4)	2.181(2)	2.187(6)	2.183(5)	2.191(5)
	2.200(3)	2.189(5)	2.180(4)	2.186(2)	2.188(6)	2.206(5)	2.205(5)
C–O	1.301(4)	1.317(8)	1.305(5)	1.293(3)	1.299(8)	1.298(9)	1.299(8)
	1.289(4)	1.301(8)	1.296(5)	1.295(3)	1.261(8)	1.285(10)	1.314(8)
C=O	1.228(4)	1.233(8)	1.224(5)	1.234(3)	1.232(9)	1.226(8)	1.245(8)
	1.253(4)	1.239(8)	1.228(6)	1.236(3)	1.265(9)	1.222(10)	1.232(8)
bond angles [°]							
O-Sn-O	82.61(9)	82.89(17)	83.77(12)	85.66(7)	87.60(19)	84.17(18)	85.47(17)
O-Sn···O_{anti}	73.56(8)	72.35(16)	72.97(13)	74.33(7)	73.49(18)	71.28(19)	73.49(16)
	72.25(8)	71.02(16)	70.24(12)	72.60(7)	73.39(18)	74.96(18)	72.10(15)
O-Sn···O_{syn}	56.59(8)	55.03(15)	54.95(13)	55.28(7)	55.17(18)	53.68(18)	56.24(16)
	52.85(8)	51.89(15)	50.76(12)	54.14(7)	53.51(18)	52.41(19)	50.81(15)
O···Sn···O	106.66(8)	105.26(15)	103.67(10)	107.98(7)	106.06(17)	106.12(18)	105.29(14)
N_i-Sn-N_i	79.19(9)	79.5(2)	78.78(14)	79.30(8)	79.2(2)	79.20(18)	79.1(2)
	79.09(9)	79.6(2)	79.66(14)	78.53(8)	78.4(2)	79.28(19)	80.0(2)
	78.58(10)	79.6(2)	78.20(14)	78.88(8)	78.2(2)	79.12(19)	79.5(2)
	77.72(9)	78.2(2)	79.74(14)	78.55(9)	78.9(2)	77.72(18)	78.1(2)
O–C=O	120.5(3)	119.46(1)	121.12(3)	120.3(3)	121.7(8)	119.9(7)	122.4(6)
	118.2(3)	118.72(1)	121.59(2)	120.9(3)	118.9(7)	120.9(7)	119.3(6)
dihedral angles [°]							
O=C-O-Sn	2.3(4), 1.4(3)	−1.1(7), 8.7(8)	4.6(5), 13.4(5)	0.6(2), −1.4(3)	−5.2(9), −0.9(7)	−0.2(9), 6.4(8)	1.7(8), 1.8(6)
N_i-N_i-N_i-N_i	4.2(2)	−4.4(2)	−4.17(17)	4.4(1)	4.32(26)	5.12(21)	−4.18(23)
2D dimensions [Å]							
N_i···N_i	3.877(3)	3.876(2)	3.881(7)	3.873(3)	3.878(8)	3.886(8)	3.913(8)
	3.913(4)	3.908(2)	3.923(5)	3.909(5)	3.883(9)	3.904(6)	3.919(7)
C_{out}···C_{out}	13.043(10)	13.067(8)	13.089(6)	13.074(4)	13.102(12)	12.992(10)	13.079(10)
	13.052(10)	13.086(9)	13.079(7)	13.070(4)	13.100(12)	13.011(10)	13.082(10)
	13.029(10)	13.040(8)	13.048(10)	13.034(6)	13.089(13)	13.008(13)	13.046(10)
	13.063(10)	13.061(8)	13.050(10)	12.997(6)	13.115(13)	13.016(13)	13.026(10)
N_4–Sn deviation [Å]	−0.773	−0.748	−0.755	−0.765	−0.769	0.766	0.755
angle between tail planes [°]	76.73(13)	46.96(13)	171.44(36)[a]	162.71(13)	107.53(42)[b]	0.95(12)	170.16(10)[c]

[a] C36, C37, and C41 were omitted in the plane calculations. [b] C36 and C38 were omitted in the plane calculations. [c] C46, C47, and C48 were omitted in the plane calculations.

O and Sn).[49] The coordination geometries surrounding the tin atoms are distorted square-antiprismatic.

The COOSn parameters obtained from the X-ray analysis confirmed the μ character of the carboxylate ligand. In previous σ-bonded COOSn fragments with pentacoordinate tin atoms,[36] the length of the C–O bond was 1.289–1.316 Å, while that of C=O bonds was 1.196–1.221 Å. In previous μ-bonded COOSn fragments[37–38] with heptacoordinate tin atoms, the length of the C=O bond was 1.227–1.241 Å, while that of C–O bonds was 1.282–1.301 Å. For compounds of type **3**, the measured C–O bond lengths were 1.261–1.317 Å, while those for the C=O bond were 1.222–1.265 Å; these values are closer to the μ-bonded COOSn fragments previously reported. The latter comparison suggests the presence of octacoordinate tin atoms in all cases, which reinforces the findings shown by the ^{119}Sn NMR and IR data.[19]

The Pc^{2-} conformations are shown in Figure 3 as follows: **3a**, **3b** and **3e** half-domed, **3a**·$CHCl_3$ and **3f** skew half-domed, and **3c-A** as well as **3c-B** ruffled.

With respect to the nanocap shape of compounds **3**, the average diameter of the Pc^{2-} moiety should be smaller than the external Pc diameter of PcH_2[50,51] (13.06–13.14 Å). An analysis of the shape of other examples of nanocap SnPcs for example, $[Pc_2Sn]$[52,53] and [PcSn],[54] shows that these have averaged external Pc diameters of 12.95 and 13.06 Å, respectively. The smaller diameter of $[Pc_2Sn^{IV}]$ can be explained by the π···π repulsive interaction of Pc···Pc, which bends the Pc ligand and makes the cavity deeper. Because $[PcSn^{II}]$ has almost the same diameter as the **3** series, it is proposed that the stereoelectronic influence of two anisobidentate $RCOO^-$ moieties is comparable to the presence of a lone pair (LP) of electrons.

The average deviation of the tin atoms from the N_4 plane in the **3** series is 0.761 Å, while $[Pc_2Sn^{IV}]$ and $[PcSn^{II}]$ have values of 1.041 and 0.903 Å, respectively. This is attributed to the high electronic repulsion between the two aromatic Pc rings, in the first case, and the coplanar Pc ring with the LP repulsive effect, in the second case.

The average $Sn–N_i$ (i = isoindolic) bond length in the **3** series, with a $Sn^{IV}O_4N_4$ core, is 2.168 Å, while that in $[Pc_2Sn]$ is 2.338 Å, which is also attributed to the π···π repulsive interactions in the $Sn^{IV}N_8$ core. $[PcSn^{II}]$, with a LP-$Sn^{II}N_4$ core, has an averaged bond length of 2.266 Å. The shorter bond lengths found in the **3** series indicate that one Pc ring and two $RCOO^-$ ligands relax the coordination sphere of the tin atom more efficiently than two Pc rings and a combination of one Pc ring and a LP. The average $C–N_i$ bond length is 1.385 Å in the **3** series, 1.369 Å for $[Pc_2Sn^{IV}]$ and 1.369 Å for $[PcSn^{II}]$, indicating the same relaxation effects. The average $C–N_{azo}$ bond length is 1.323 Å in the **3** series, 1.320 Å for $[Pc_2Sn^{IV}]$ and 1.332 Å for $[PcSn^{II}]$, denoting that the azo bridges are no longer deformed.

At the supramolecular level, there are significant changes. They are mainly caused by solvent–Pc, Pc–Pc hydrogen bonds, π···π and σ···π interactions, and partial overlapping of the Pc ligands. They are also affected by the conformations of the hydrocarbon tails. The supramolecular arrays in the **3** series are discussed below.

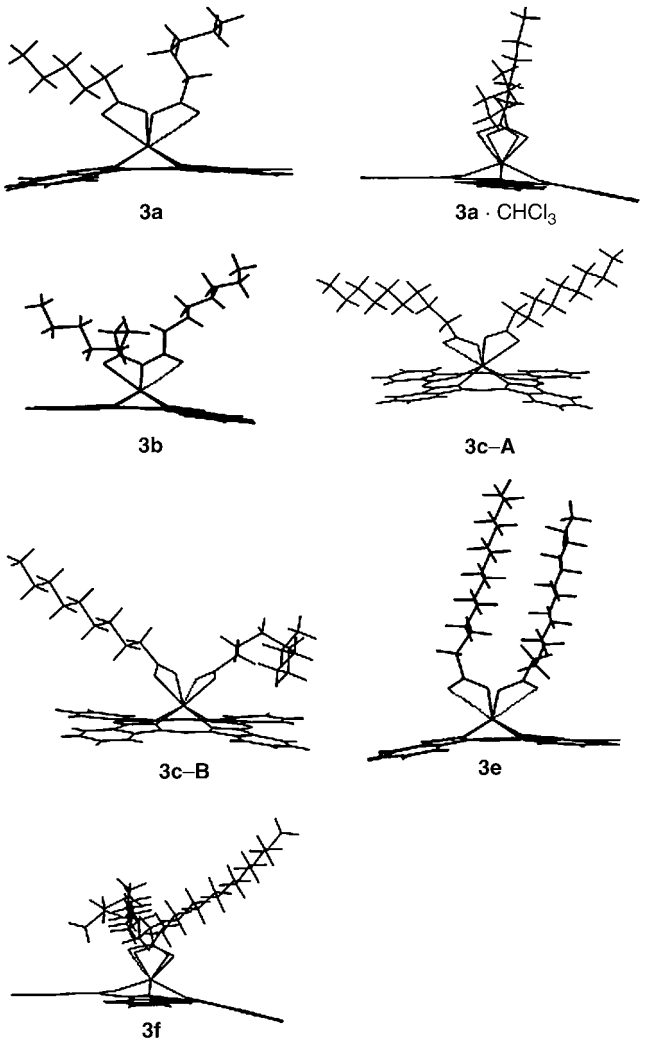

Figure 3. Pc conformation for **3a** (half-domed), **3a**·$CHCl_3$(skewed half-domed), **3b**(half-domed), **3c-A**(ruffled), **3c-B**(ruffled), **3e** (half-domed), and **3f**(skewed half-domed).

Compound **3a** can crystallize as two allotropes, **3a** and **3a**·$CHCl_3$, whereby the latter contains solvent. Polymorph **3a** presents a partial concave 2/3 overlap of the Pc ligands. One hydrocarbon tail is positioned perpendicularly to the Pc plane, while the other is parallel to it, resulting in a tail plane–tail plane angle of 76.73(13)°. There are four, two-fold symmetry-related, π···π contacts, exhibiting distances of d(C2–C23) = 3.396, d(C1–C24) = 3.145, d(C8–C25) = 3.184 and d(C17–C32) = 3.234 Å. There are three types of hydrogen bonding, $d(C_{ar}–H_{inner}···O–C=O)$ = 2.402 and two $d(C_{aliph}–H···O–C=O)$ = 2.478, 2.661 Å. These structural factors are combined into a partial cyclophane-type arrangement. Polymorph **3a**·$CHCl_3$ presents a hydrogen bond of the type $d(Cl_3C–H···O···Sn)$ = 2.189 Å, increasing the Sn···O bond length (d(PcSn···O=C) = 2.757(5) Å, normal d-(PcSn···O=C) = 2.543(5) Å). This compound presents a partial concave 2/3 overlap of the Pc ligands. One hydrocarbon

tail is positioned perpendicularly to the Pc plane, while the other is parallel to it and this results in a tail plane–tail plane angle of 46.96(13)°. There are also four, twofold symmetry-related, π···π contacts, exhibiting distances of *d*(C25–N1) = 3.191, *d*(C1–C24) = 3.271, *d*(C2–C23) = 3.281 and *d*(C13–C16) = 3.281 Å, and two hydrogen bonds of *d*(C_{ar}–H_{inner}···O–C=O) = 2.402 and *d*(C_{ar}–H_{outer}···O–C=O) = 2.517 Å in magnitude, denoting a closed packing structure for the inner hydrogen.

Compound **3b** presents a convex 1/3 overlap of the Pc in one direction and a concave 2/3 overlap in the other. There are four, twofold symmetry-related, π···π contacts, exhibiting distances of *d*(C5–C13) = 3.277, *d*(C6–C12) = 3.284, *d*-(C20–C29) = 3.255 and *d*(C32–C32) = 3.397 Å, and two hydrogen bonds of *d*(C_{ar}–H_{outer}···O=C-O) = 2.425 and *d*-(C_{ar}–H_{outer}···O–C=O) = 2.591 Å. The conformation of the hydrocarbon tails is *anti* oriented, with a tail plane–tail plane angle of 171.44(36)°. One chain is straight and the other is helicoid because of the strain of a Pc neighbor.

Compound **3c** can also crystallize as two allotropes, but without solvent co-crystallization, namely **3c-A** and **3c-B**. DFT calculations were performed on both **3c** polymorphs at the PW91/GGA level of theory.[55] The theoretical results indicated that both conformers are almost isoenergetic ($\Delta E_{(\mathbf{3c\text{-}A-3c\text{-}B})}$ = 0.0033 eV, 0.076 kcal mol^{-1}) taking into account the full 3D crystallographic cell and its contents, see the Supporting Information for further details. Polymorph **3c-A** has a ruffled conformation on account of a convex 1/3 overlap of the Pc ligands in one direction and a concave 2/3 overlap in the other. There are five, twofold symmetry-related, π···π contacts, exhibiting distances of *d*(C25–N1) = 3.335, *d*(C1–C24) = 3.359, *d*(C17–C32) = 3.397, *d*(N1–C24) = 3.185, and *d*(C7–C26) = 3.308 Å, and two hydrogen bonds of *d*(C_{ar}–H_{outer}···O–C=O) = 2.597 and *d*(C_{ar}–H_{outer}···O=C-O) = 2.697 Å. These structural factors are combined into a cyclophane-type arrangement. The hydrocarbon tails are *anti* oriented, with a tail plane–tail plane angle of 162.71(13)°; this phenomena results from the accommodation of hydrophobic moieties. Another contact was encountered in a conformation analysis of the tail, namely, a hydrogen bond with *d*(C–H···N_{azo}) = 2.689 Å, which fixes the tail packing more rigidly. Polymorph **3c-B** has a ruffled conformation on account of a convex 1/3 overlap of the Pc ligands in one direction and a concave 2/3 overlap in the other. In this case, there are six, twofold symmetry-related, π···π contacts, exhibiting distances of *d*(C20–C29) = 3.182, *d*(C5–C11) = 3.284, *d*-(C5–C12) = 3.363, *d*(C12–C22) = 3.339, *d*(C4–C13) = 3.325. and *d*(C13–C21) = 3.365 Å, and two hydrogen bonds of *d*(C_{ar}–H_{outer}···O=C-O) = 2.417 and *d*(C_{ar}–H_{outer}···O–C=O) = 2.515 Å. The result of both H···O bonds is the construction of an isoindoline-bridged moiety in the shape of a fully overlapped cyclophane at the six carbon atoms of the aromatic fragment. The hydrocarbon tails are *anti* oriented, with a tail plane–tail plane angle of 107.53(43)°. Another contact was encountered in a conformation analysis of the tail, namely, a hydrogen bond with *d*(C–H···N_{azo}) = 2.719 Å is present, which rigidly fixes the tail.

Compound **3e** exhibits a convex 2/3 overlap of the Pc ligands in one direction and also a concave 2/3 overlap in the other. In this case, there are four, twofold symmetry-related, π···π contacts, exhibiting distances of *d*(C1–C13) = 3.178, *d*-(C7–C14) = 3.376, *d*(C8–C14) = 3.349, and *d*(C10–C21) = 3.366 Å, and one hydrogen bond of *d*(C_{ar}–H_{inner}···O–C=O) = 2.358 Å. The hydrocarbon tails are *syn* oriented, with a tail plane–tail plane angle of 0.95(12)°.

Compound **3g** presents a convex 1/3 overlap of the Pc ligands in one direction and a concave 2/3 overlap in the other. There are five, twofold symmetry-related, π···π contacts, exhibiting distances of *d*(N1–C24) = 3.184, *d*(C8–C24) = 3.364, *d*(C8–C25) = 3.384, *d*(C7–C25) = 3.293, and *d*(C7–C26) = 3.342 Å, and two hydrogen bonds of *d*-(C_{ar}–H_{outer}···O–C=O) = 2.616 and *d*(C_{ar}–H_{outer}···O=C-O) = 2.633 Å that improve the cyclophane shape. The hydrocarbon tails are *anti* oriented, with a tail plane–tail plane angle of 170.16(10)°.

Figure 4 depicts samples of the supramolecular contacts discussed above.

At this point, it is worth mentioning that, as in the case of tin(IV) systems, soluble species are obtained from axial substitution reactions of [PcTi=O], [$PcTiCl_2$], and [PcGaX] (X = halogen) systems (also nanocap shaped).[56] The literature cited for [PcTi] and [PcGa] moieties is directly related to their use in nonlinear optic (NLO) properties.[56a] Hence, according to the molecular design outlined for NLO applications, the [PcSn] systems may also be suitable for these applications and further work is under study.

Electrochemical testing and corrosion inhibitor measurements: Compounds **3a–h** were tested as corrosion inhibitors for carbon steel in naturally aerated brine saturated with H_2S, to measure the protection of steel against sour corrosion (see the Supporting Information for details). A corrosion rate of about 81.8 mpy was determined on carbon steel AISI 1018 before iron sulfide formation. However, the steady-state corrosion rate after 2–3 h in the sour environ-

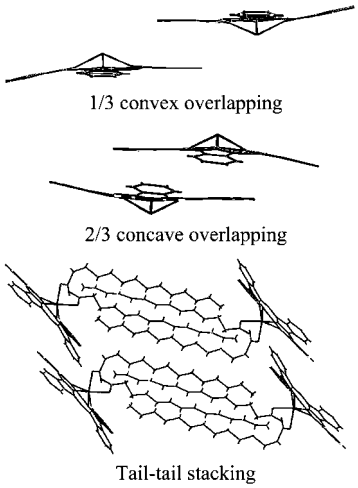

Figure 4. Supramolecular interactions observed for **3** series.

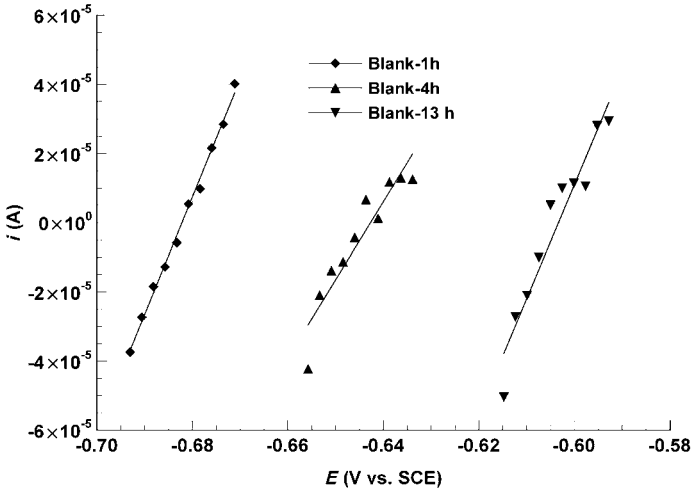

Figure 5. Polarization curves of carbon steel AISI 1018 in sour brine without inhibitor that show an increase in electrode potential to more anodic values with testing time.

ment may decrease to about 50 mpy as derived from the sulfide film formation. Instantaneous and steady-state corrosion rates of the blank material were determined by the Linear Polarization Resistance (LPR) technique to avoid damaging the metallic surface. Polarization scans of AISI 1018 in sour brine in the presence of inhibitors **3a–h** displayed corrosion rates of 20–82 mpy, with corrosion inhibition efficiencies ranging from 40–85 %.[57,58]

An example of the LPR results on steel blanks is depicted in Figure 5. The polarization resistance increases as the testing time increases, while a reduction in the testing current is observed. This behavior is attributed to the formation of iron sulfide over the metallic surface. However, the displacement of the electrode potential to more anodic values with increasing testing time indicates that there is a tendency for the corrosion process to resume.

A corrosion rate of about 81.75 mpy was determined on a clean blank surface after a period of 3 min, while the corrosion rate of about 50 mpy is related to the blank sample in sour brine after 2–3 h of exposure. In both cases, the sample was left to rest at the open circuit potential (OCP) before electrochemical testing. The instantaneous corrosion rate on the blank material agrees well with that reported for carbon steel AISI 1017 in sour brine.[59]

Table 4 depicts the inhibition efficiency after 5 h obtained from a comparison of a clean blank surface and those of inhibited ones. Compounds **3a–h** displayed an efficiency of 58.8–86.7 %, which suggests that the nanocap morphology permits an effective absorption at the concentrations applied for this study. However, the measured efficiencies do not follow a defined pattern and this may be because of the lack of film resistance and fluid aggressiveness. Although there is no clear relationship between the inhibitor efficiency and the hydrocarbon tail length, the evidence suggests that long tails in combination with double bonds may result in an improved inhibitor activity (e.g. stearic acid derivative **3g** versus oleic acid derivative **3h**). The best results, are 85.3 % (**3e**) and 78.7 % (**3h**) at a concentration of 1000 ppm, and 85.3 (**3e**) and 86.71 (**3h**) at 500 ppm.

Table 4. Corrosion inhibitor efficiency[%] of **3a–h** tested in for carbon steel in sour brine.

Compound	Carbon length	Efficiency[%]		
		1000 ppm	500 ppm	300 ppm
3a	C6	74.5	73.9	[a]
3b	C8	75.8	75.3	[a]
3c	C10	58.8	74.1	[a]
3d	C12	72.3	60.5	[a]
3e	C14	85.7	85.3	[a]
3f	C16	67.6	65.5	[a]
3g	C18	64.1	67.9	[a]
3h	C18, double bond	78.7	86.7	64.67

[a] Not determined.

The corrosion inhibitor efficiency found for compounds **3a–h** may be attributed to a parallel-oriented chemisorption of the nanocap metal complexes at the steel surface, whereby the absorption phenomena involve charge transfer from the inhibitor molecule to the metallic surface, so that the efficiency of these compounds depends on the number of active acidic centers that are covered by the nanocap surface, which ranges from 1076 $Å^2$ (**3a**) to 1769 $Å^2$ (**3g**) for the chemisorption.

The molecular design is understood in the sense that the π-electron-rich nanocap surface permits adsorption, while the length of the carbon tail promotes hydrophobic protection towards the deposition of contaminants over the steel surface. On the other hand, inhibitors with a relatively short carbon tail display a more uniform behavior in the absence of a double bond at the carboxylic moiety, namely, an increase in corrosion efficiency with carbon chain length, which can be more clearly observed when these inhibitors ($C < 12$) are compared at different concentrations.

A summary of the relevant electrochemical data derived from the use of **3e** and **3h** inhibitors is presented in Table 5. Figure 6 provides an example of the effect of **3h** in sour brine because it is the most soluble compound of the series.

Table 5. Electrochemical data for **3e** and **3h** inhibitors at 500 ppm.

Corrosion inhibitor	Blank material	**3e**	**3h**
Rp [ohm]	2.78×10^{2}	1.214×10^{3}	2.073×10^{3}
I_{corr} [A]	9.18×10^{-5}	5.77×10^{-5}	1.192×10^{-5}
E_{corr} [V versus SCE]	−0.51	−0.69	−0.69
efficiency [%]	0.00	67.9	86.7

As a general tendency, is worth noting that the current density is decreased as the inhibitor concentration is increased in the fluid. Additionally, it is observed that **3h** abates both the anodic and the cathodic curve branches and displaces the equilibrium potential to more cathodic values thereby producing a considerable inhibitive effect.

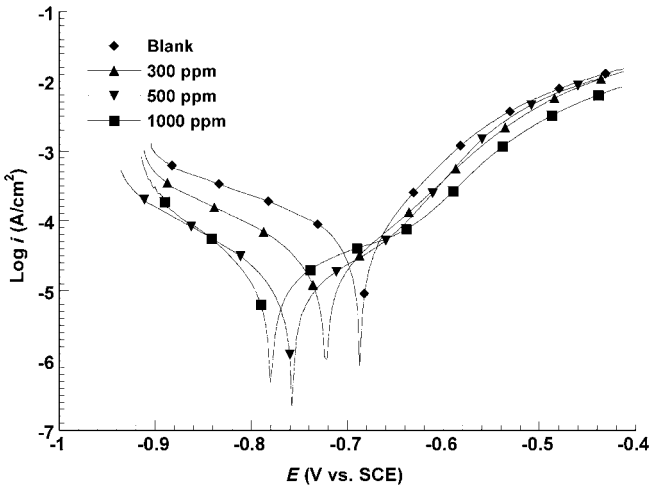

Figure 6. Polarization curves of carbon steel AISI 1018 in sour brine with oleic inhibitor **3h** at the concentrations indicated after one hour at OCP. The current density decreases as the the inhibitor concentration increases.

Conclusion

trans-Phthalocyanine–tin(IV) dichloride can be transformed in high yields to *cis*-phthalocyanine–tin(IV) dicarboxylates by means of thermal and microwave treatments. The reaction rates of the MW syntheses are about 15 times faster than those of the thermal procedure. The optimized reaction conditions for the MW process are 5 min of exposure and 600-W microwave power.

The anisobidentate binding mode of the COOSn fragments give rise to IR bands at lower wavenumbers than those known for normal σ-COOSn binding modes. The coordination number was confirmed by the determination of seven X-ray structures of *cis*-phthalocyanine–tin(IV) dicarboxylates, which revealed octacoordinated tin atoms with a square-antiprismatic coordination geometry linked to the asymmetrically bonded COOSn moieties.

The ^{1}H and ^{13}C NMR spectra revealed that the ring currents in the Pc^{2-} ligands affect the chemical shift up to the fifth methylenic position, while the spin rotational relaxation mechanism is diminished mainly for the α-methylene position. The ^{119}Sn NMR chemical shift values were indicative of octacoordinate tin(IV) atoms in solution.

The supramolecular contacts of the crystallographic lattices consist of π···π, σ···π, N_{azo}···H–C_{ar}, O–C=O···H–C_{ar}, and O=C-O···H–C_{ar} interactions. As these intermolecular interactions modify the conformations of the aliphatic backbones and induce different types of deformation in the Pc ligands, they have a significant effect on the molecular packing, which in turn affects the inhibitor efficiency. Apparently, long tails in conjunction with double bonds in the hydrocarbon tail have a faster and more efficient inhibition effect.

The measurements of the corrosion rate indicate that compounds of type **3** can act as corrosion inhibitors at concentrations of about 500 ppm. The compounds **3e** and **3h** exhibited the best performance with efficiencies ranging between 78.7 and 86.7%. A full set of experiments performed at different concentrations of **3h** indicates that the corrosion inhibition efficiency is a function of inhibitor concentration.

Experimental Section

Fatty acids, dicyanobenzene, dichlorotin(II) dihydrate, potassium bicarbonate and quinoline were purchased from Aldrich Co. DMF and chloroform solvents were purchased as reagent grade from Fermont Co. Quinoline was distilled before use. All reactions and operations were carried out under atmospheric conditions.

Instrumentation: NMR experiments were performed on VARIAN Mercury200 and VARIAN Mercury200-BB spectrometers. ^{1}H and ^{13}C chemical shifts are relative to internal $SiMe_4$ (TMS) and ^{119}Sn chemical shifts are relative to $SnMe_4$. The microwave reactions were performed on a focused ESEV model Mic1 microwave reactor provided with digital control and a power of 100–600 W. The IR spectra were recorded in the range of 400–4000 cm^{-1} on a Bruker Tensor-27 FT-IR spectrometer as KBr pellets. UV/Vis spectra were obtained on a Lambda35 Perkin–Elmer Spectrometer. Elemental analyses were obtained on a CHNO/S Perkin–Elmer analyzer.

Preparation of the fatty acid salts: General procedure to prepare **2a**: A mixture of hexanoic acid (**1a**, 5.0 g, 43 mmol), potassium bicarbonate (4.3095 g, 43 mmol), and reagent-grade methanol (50 mL) in a 100 mL flask was refluxed for 2 h. The solvent then was removed under reduced pressure and the remaining substance was washed (3×10 mL chloroform/*n*-heptane) to afford **2a** as a white amorphous solid. Yield: 6.5125 g (42 mmol, 98.1%).

Equimolecular quantities of starting materials gave compounds **2b–h** in yields of 64% (**2b**), 97% (**2c**), 86% (**2d**), 81% (**2e**), 83% (**2f**), 99% (**2g** and 88% (**2h**).

Preparation of compounds 3a–h by the thermal procedure: *General procedure for compound **3a***: [Cl_2SnPc] (**1**, 0.5 g, 7 mmol) and **2a** (0.2198 g, 14 mmol) were added to DMF (25 mL) in a 100-mL reaction flask, and the reaction mixture was refluxed 2.5 h. After completion of the reaction, the product was filtered and washed with chloroform (3×20 mL) to extract the final compound. After removing the solvent under reduced pressure, the remaining powder was washed with methanol (3×50 mL) to afford **3a** as a dark blue solid. Yield: 0.33 g (4 mmol, 54%). M.p.< 300°C; IR (KBr): $\tilde{\nu}$ = 2954, 2927, 2856, 1609, 1503, 1466, 1421, 1332, 1287 cm^{-1}; UV (EtOH): λ = 210, 252, 360, 616, 682 nm; elemental analysis calcd (%) for $C_{44}H_{40}N_8O_4Sn$: C 61.20, H 4.67, N 12.98; found: C 61.30, H 4.73, N 13.07. Crystals of **3a** were grown by slow cooling of the crude reaction mixture. Crystals of **3a**·$CHCl_3$ were obtained by dissolving **3a** in chloroform/hexane (1:2) and leaving for one week.

*Compound **3b***: Blue deep solid; yield: 55%; m.p. 257–259°C; IR (KBr): $\tilde{\nu}$ = 2924, 2854, 1608, 1502, 1466, 1421, 1332, 1287, 1118, 1079, 893, 727 cm^{-1}; UV (EtOH): λ = 212, 253, 360, 616, 682 nm; elemental analysis calcd (%) for $C_{48}H_{48}N_8O_4Sn$: C 62.69, H 5.26, N 12.18; found: C 62.41, H 5.18, N 12.34. Crystalline material was obtained after recrystallization of **3b** from a 1:4 mixture of dichloromethane and hexane.

*Compound **3c***: Blue crystalline solid; yield: 58%; m.p. 246–247°C; IR (KBr): $\tilde{\nu}$ = 2921, 2851, 1609, 1503, 1467, 1421, 1333, 1288, 1119, 1080, 873, 750, 727 cm^{-1}; UV (EtOH): λ = 213, 360, 616, 682 nm; elemental analysis calcd (%) for $C_{52}H_{56}N_8O_4Sn$: C 64.01, H 4.67, N 12.98; found: C 64.24, H 4.78, N 13.07. Single crystals suitable for X-ray studies were grown by slow evaporation of a saturated solution of **3c** in chloroform.

*Compound **3d***: Deep blue crystalline solid; yield: 78%; m.p. 229–231°C; IR (KBr): $\tilde{\nu}$ = 2922, 2852, 1609, 1586, 1502, 1467, 1422, 1333, 1289, 1119, 1080, 895, 728 cm^{-1}; UV (EtOH): λ = 205, 254, 360, 616, 682 nm; elemental analysis calcd (%) for $C_{56}H_{64}N_8O_4Sn$: C 65.18, H 6.25, N 10.66; found: C 65.00, H 6.18, N 10.50.

*Compound **3e***: Deep blue crystalline powder; yield: 63%; m.p. 214–215°C; IR (KBr): $\tilde{\nu}$ = 2916, 2849, 1609, 1499, 1463, 1418, 1328, 1294,

1114, 1073, 719 cm^{-1}; UV (EtOH): λ = 212, 253, 360, 616, 682 nm; elemental analysis calcd (%) for $C_{60}H_{72}N_8O_4Sn$: C 66.24, H 6.67, N 10.30; found: C 66.02, H 6.54, N 10.18.

Compound ***3f***: Blue powder; yield: 78%; m.p. 229–231°C; IR (KBr): $\tilde{\nu}$ = 2921, 2851, 1609, 1503, 1467, 1422, 1333, 1288, 1119, 1080, 895, 775, 750, 728 cm^{-1}; UV (EtOH): λ = 212, 253, 360, 616, 682 nm; elemental analysis calcd (%) for $C_{64}H_{80}N_8O_4Sn$: C 67.19, H 7.05, N 9.79; found: C 67.08, H 6.94, N 9.92.

Compound ***3g***: Blue powder; yield: 66%; m.p. 199–201°C; IR (KBr): $\tilde{\nu}$ = 2919, 2850, 1609, 1503, 1467, 1422, 1333, 1289, 1078, 894, 726 cm^{-1}; UV (EtOH): λ = 214, 359, 619, 682 nm; elemental analysis calcd (%) for $C_{68}H_{88}N_8O_4Sn$: C 68.05, H 7.39, N 9.34; found: C 67.88, H 7.42, N 9.48.

Compound ***3h***: Blue powder; yield: 62%; m.p. 189–191°C; IR (KBr): $\tilde{\nu}$ = 2919, 2850, 1609, 1503, 1467, 1422, 1333, 1289, 1078, 894, 726 cm^{-1}; UV (EtOH): λ = 214, 359, 619, 682 nm; elemental analysis calcd (%) for $C_{68}H_{84}N_8O_4Sn$: C 68.28, H 7.08, N 9.37; found: C 68.10, H 6.98, N 9.30.

Preparation of compounds 3a–h using a MW procedure: *General procedure for compound* ***3a***: Compound **1** (0.5 g, 7 mmol) and compound **2a** (0.2198 g, 14 mmol) were dissolved in DMF (20 mL) and the solution was heated for 5 or 10 min in the microwave reactor with a power supply of 300 W or 600 W, respectively, at a set up temperature of 150°C. The purification procedure followed was the same as that used in the thermal procedure. The resultant yields under the different operational conditions are given in Table 1.

In the case of compounds **3c** and **3f**, single crystals suitable for X-ray crystallography were grown by slow cooling of the MW reaction media. In the case of **3c**, mixtures of two different polymorphs were obtained, **3c-A** and **3c-B**.

X-ray crystallography: X-ray diffraction studies of **1**, **3a**, **3a**·$CHCl_3$, **3b**, **3c-A**, **3c-B**, **3e**, and **3f** were carried out on a Bruker-AXS APEX diffractometer with a CCD area detector ($\lambda_{MoK\alpha}$ = 0.71073 Å, monochromator: graphite). Frames were collected at T = 100 K or 298 K with ω and ϕ rotation at 10 s per frame (SMART[60]). The measured intensities were reduced to F^2 and corrected for absorption with SADABS (SAINT-NT[61]). Structure solution, refinement, and data output were carried out with the SHELXTL-NT program package.[62] Non-hydrogen atoms were refined anisotropically. For the study of **3e**, an Enraf-Nonius FR590 Kappa-CCD diffractometer ($\lambda_{MoK\alpha}$ = 0.71073 Å, monochromator: graphite, T = 298 K) was used. In this case, the SHELXS-97[63] program was applied for the structure solution, while the SHELXL-97[63] was used for refinement and data output. All data were corrected for Lorentz and polarization effects. All additional measurements were carried out with the WINGX[64] program set with the PARST[65] utility; the corresponding molecular graphs were prepared with the ORTEP 3[66] and Mercury 1.2[67] programs.

CCDC-256307–CCDC-256311 contain the supplementary crystallographic data for this paper. These data can be obtained free of charge from The Cambridge Crystallographic Data Centre via www.ccdc.cam.ac.uk/data_request/cif.

Sour brine preparation: NaCl (60 g), $CaCl_2{\cdot}2H_2O$ (6.62 g), $MgCl_2{\cdot}6H_2O$ (10.65 g), and Na_2SO_4 (3.5 g) were dissolved in distilled water (1 L) and mixed with an external impeller until the salt had completely dissolved. The mixture was poured into a double-wall reactor. The solution was cooled to 5±1°C in a recirculating bath, which continuously pumped tap water through the outer wall of the reactor. Nitrogen was injected over a period of 40 min at a rate of 5.5–7.0 L min^{-1} to remove oxygen. The nitrogen flow was stopped and hydrogen sulfide was injected at a rate of 0.4–0.5 L min^{-1} for the period required (≈30 min) to reach a pH of 4±0.3. The sour brine was then deposited in the previously used vessel. On account of the harmfulness of H_2S to human health, the sour brine was prepared in an aerated hood; after every set of electrochemical tests, this solution was put into an industrial freezer to avoid loss of H_2S. Fresh sour brine was prepared every day for the duration of the tests.

Preparation of the 3a–h inhibitor solutions: For each inhibitor, a 10000 ppm solution was prepared from 1.00 g of inhibitor powder, which was dissolved with chloroform and then stirred for a period of 10 min to accomplish dissolution. Depending on the inhibitor concentration required, a proportional volume of inhibitor was calculated, and then deposited in a 100-mL volumetric flask that was filled up with sour brine. Solutions with 300, 500, and 1000 ppm were prepared from each of the reported corrosion inhibitors. The solutions were then poured into electrochemical cells (100 mL) for electrical contact.

Electrode preparation: The specimens consisted of carbon steel of the type AISI 1018 with the composition C = 0.14–0.20%, Si = 0–40 to 0–50%, Mn = 0.60–0.90%, P = 0.030% max., S = 0.035% max, Fe = remainder. Samples were machined from a round bar of 12.5 mm diameter to obtain a 0.5 cm^2 cross-sectional area. Carbon steel specimens were inserted into rigid Teflon caps; the metal/Teflon interface was sealed with epoxy resin to avoid localized corrosion. Teflon caps were previously threaded to adjust a metallic extension for electrochemical testing.

Working electrode samples were grounded with a 600# grit SiC paper surface finish, washed with distilled water, rinsed in acetone, and dried before being exposed to the aqueous test environments. The electrolyte was the sour brine solution.[68] Electrochemical testing was performed at room temperature (20–25°C) in naturally aerated and inhibited sour brine solutions.

Electrochemical corrosion measurements were performed with a potentiostat-galvanostat Autolab 30 and monitored by the GPES[69] set of programs installed on a Pentium III computer. A three-electrode system was employed, that consisted of an auxiliary graphite counterelectrode, a saturated calomel reference electrode (SCE), and the test material as the working electrode. The volume of the cell was 100 mL and no deaeration was provided.

Linear polarization resistance tests were performed at a scan rate of 0.16 mV s^{-1} on clean sample surfaces, to determine the instantaneous corrosion rate before ferrous sulfide formation. Testing was also performed at intervals of 60 min during 24 h to define the steady state of the corrosion rate of steel in sour brine. These tests were made with a salt bridge to avoid contamination by mercurous sulfide. Polarization curves were performed within ±250 mV (versus OCP) at a scan rate of 0.5 mV s^{-1}. Corrosion rates were determined by the Faraday law for the LPR technique and by Tafel slope extrapolation analysis for the polarization scans.[70]

Acknowledgement

The present study was supported by the Instituto Mexicano del Petróleo, Programa de Ingeniería Molecular (Project No. D.00178).

[1] F. H. Moser, A. L. Thomas, *Phthalocyanine Compounds*, Reinhold Publishing Corp. (New York) **1963**, p. 2.
[2] H. Engelkamp, S. Middelbeek, R. M. J. Nolte, *Science* **1999**, *284*, 785–788.
[3] J. L. Brédas, C. Adant, C. Tackx, A. Persoons, *Chem. Rev.* **1994**, *94*, 243–278.
[4] N. Kobayashi, *Coord. Chem. Rev.* **2002**, *227*, 129–152.
[5] H. B. Wang, L. S. Wang, *Nature* **1999**, *400*, 245–248.
[6] B. Crone, A. Bodabalapur, Y. Y. Lin, R. W. Filas, Z. Bao, L. A. LaDuca, R. Sarpeshkar, H. E. Katz, W. Li, *Nature* **2000**, *403*, 521–523.
[7] Phillips Research CNRS, News Feature, *Nature* **2000**, *407*, 442–444.
[8] Q. M. Zhang, H. Li, M. Poh, X. Feng, Z. Y. Cheng, H. Xu, C. Huang, *Nature* **2002**, *419*, 284–287.
[9] M. A. Baldo, D. F. O'Brien, Y. You, A. Shoustikov, S. Sibley, M. E. Thompson, S. R. Forrest, *Nature* **1998**, *395*, 151–154.
[10] N. Kobayashi, *Coord. Chem. Rev.* **2001**, *219–221*, 99–123.
[11] C. C. Leznoff, A. B. P. Lever, *Phthalocyanines: Properties and Applications*, *Vol. 1–4*, Wiley, New York, **1989–1996**.
[12] M. K. Engel, *Kawamura Rikagaku Kenkyusho Hokoku* **1997**, *8*, 11–54.

[13] C. G. Claessens, D. González-Rodríguez, T. Torres, *Chem. Rev.* **2002**, *102*, 835–853.
[14] T. Fukuda, J. R. Stork, R. J. Potucek, M. M. Olmstead, B. C. Noll, N. Kobayashi, W. S. Durfee, *Angew. Chem.* **2002**, *114*, 2677–2680; *Angew. Chem. Int. Ed.* **2002**, *41*, 2565–2568.
[15] T. Fukuda, M. M. Olmstead, W. S. Durfee, N. Kobayashi, *Chem. Commun.* **2003**, 1256–1257.
[16] K. Schweiger, M. Göldner, H. Hückstädt, H. Homborg, *Z. Anorg. Allg. Chem.* **1999**, *625*, 1693–1699.
[17] K. Schweiger, H. Hückstädt, H. Homborg, *Z. Anorg. Allg. Chem.* **1998**, *624*, 44–50.
[18] H. Hückstädt, A. Tutaß, M. Göldner, U. Cornelissen, H. Homborg, *Z. Anorg. Allg. Chem.* **2001**, *627*, 485–497.
[19] A. Tutaß, M. Klöpfer, H. Hückstädt, U. Cornelissen, H. Homborg, *Z. Anorg. Allg. Chem.* **2002**, *628*, 1027–1044.
[20] D. A. Fletcher, R. F. McMeeking, D. Parkin, *J. Chem. Inf. Comput. Sci.* **1996**, *36*, 746–747. The United Kingdom Chemical Database Service.
[21] F. H. Allen, O. Kennard, *Chemical Design Automation News* **1993**, *8*, 1 and 31–37. 3D Search and Research using the Cambridge Structural Database.
[22] M. Larhed, C. Moberg, A. Hallberg, *Acc. Chem. Res.* **2002**, *35*, 717–727.
[23] K. Tanaka, F. Toda, *Chem. Rev.* **2000**, *100*, 1025–1074.
[24] N. F. K. Kaiser, U. Bremberg, M. Larhed, C. Moberg, A. Hallberg, *Angew. Chem.* **2000**, *112*, 3741–3744; *Angew. Chem. Int. Ed.* **2000**, *39*, 3595–3598.
[25] C. R. Strauss, *Angew. Chem.* **2002**, *114*, 3741–3742; *Angew. Chem. Int. Ed.* **2002**, *41*, 3589–3591.
[26] N. Elander, J. R. Jones, S. Y. Liu, S. Stone-Elander, *Chem. Soc. Rev.* **2000**, *29*, 239–249.
[27] A. Khalafi-Nezhad, M. N. S. Rad, G. H. Hakimelahi, *Helv. Chim. Acta* **2003**, *86*, 2396–2403.
[28] S. Sharma, S. K. Sunkara, *J. Am. Chem. Soc.* **2002**, *124*, 12288–12293.
[29] D. Villemin, M. Hammadi, M. Hachemi, N. Bar, *Molecules* **2001**, *6*, 831–844.
[30] M. D. Maree, T. Nyokong, *J. Chem. Res. Synop.* **2001**, 68–69.
[31] A. Shaabani, *J. Chem. Res. Synop.* **1998**, 672–673.
[32] L. C. Liu, C. C. Lee, A. T. Hu, *J. Porphyrins Phthalocyanines* **2001**, *5*, 806–807.
[33] D. A. Davies, C. Schnik, J. Silver, J. L. Sosa-Sánchez, P. G. Riby, *J. Porphyrins Phthalocyanines* **2001**, *5*, 376–380.
[34] K. S. Jung, J. Y. Ro, J. Y. Lee, S. S. Park, *J. Mater. Sci. Lett.* **2001**, *20*, 2203–2205.
[35] a) V. S. Sastri, *Corrosion Inhibitors Principles and Applications*, Wiley, **1998**, p. 950 b) O. L. Riggs, Jr., *Corrosion Inhibitors* (Ed.: C. C. Nathan), NACE (Houston TX), **1979**, p. 265. Library Congress, Catalog No. 73-85564.
[36] H. I. Beltrán, L. S. Zamudio-Rivera, T. Mancilla, R. Santillan, N. Farfán, *Chem. Eur. J.* **2003**, *9*, 2291–2306.
[37] R. García-Zarracino, J. Ramos-Quiñones, H. Höpfl, *Inorg. Chem.* **2003**, *42*, 3835–3845.
[38] R. García-Zarracino, H. Höpfl, *Angew. Chem.* **2004**, *116*, 1533–1537; *Angew. Chem. Int. Ed.* **2004**, *43*, 1507–1511.
[39] J. Silver, C. S. Frampton, G. R. Fern, D. A. Davies, J. R. Miller, J. L. Sosa-Sanchez, *Inorg. Chem.* **2001**, *40*, 5434–5439.
[40] J. Silver, J. L. Sosa-Sanchez, C. S. Frampton, *Inorg. Chem.* **1998**, *37*, 411–417.
[41] D. A. Davies, C. Schnik, J. Silver, J. L. Sosa-Sanchez, P. G. Riby, *J. Porphyrins Phthalocyanines* **2002**, *6*, 198–202.
[42] L. S. Zamudio-Rivera, A. Estrada, A. Benavides, J. L. Benítez, *Rev. Soc. Quim. Mex.* **2002**, *46*, 335–340.
[43] L. S. Zamudio-Rivera, *Corrosion Inhibitors for Acidic Media.* PIMCQA-IMP *Mex. Pat*. **2001**, 4.
[44] H. I. Beltran, R. Esquivel, A. Sosa-Sánchez, J. L. Sosa-Sánchez, H. Höpfl, V. Barba, N. Farfán, M. Galicia-García, O. Olivares-Xometl, L. S. Zamudio-Rivera, *Inorg. Chem.* **2004**, *43*, 3555–3557.
[45] S. J. Lin, T. N. Hong, J. Y. Tung, J. H. Chen, *Inorg. Chem.* **1997**, *36*, 3886–3891.
[46] Single crystals suitable for X-ray diffraction analysis were obtained and the data is similar to that reported by Janczak.[47] Chemical formula: $C_{32}H_{16}Cl_2N_8Sn$, FW = 702.12, collection temperature: 100 K, triclinic crystal system, space group $P\bar{1}$, a = 7.2049(8), b = 8.6252(9), c = 11.0058(12) Å, α = 74.309(2), β = 80.148(2), γ = 84.681(2)°, V = 647.97(12) Å^3, Z = 1, ρ_{calcd} = 1.799 mg m^3, μ = 1.235 mm^{-1}, collection temperature 100 K, $F(000)$ = 348, crystal size 0.12 × 0.1 × 0.1 mm^3, θ range for data collection 1.94 to 27.54°, 7558 collected reflections, 2937 independent reflections [R(int) = 0.0785], completeness to θ = 27.54° (97.9%), absorption correction, SADABS, refinement method, full-matrix least-squares on F^2, data/restraints/parameters, 2937/0/220, goodness-of-fit on F^2 1.026, final R indices [$I > 2\sigma(I)$], $R1$ = 0.0580, $wR2$ = 0.1085, R indices (all data), $R1$ = 0.0749, $wR2$ = 0.1167, largest diff. peak and hole, 1.627 and −0.673 e Å^{-3}. CCDC-256734 contains the supplementary crystallographic data for this paper. These data can be obtained free of charge from The Cambridge Crystallographic Data Centre via www.ccdc.cam.ac.uk/data_request/cif.
[47] J. Janczak, R. Kubiak, *Acta Crystallogr. Sect. C* **2003**, *59*, m237 m240.
[48] R. S. Osborn, *Ph.D. Thesis*, University of London, **1973**, *3*.
[49] A. Bondi, *J. Phys. Chem.* **1964**, *68*, 441–451.
[50] P. Zugenmaier, T. L. Bluhm, Y. Deslandes, W. J. Orts, G. K. Hamer, *J. Mater. Sci.* **1997**, *32*, 5561–5568.
[51] R. B. Hammond, K. J. Roberts, R. Docherty, M. Edmondson, R. Gairns, *J. Chem. Soc. Perkin Trans. 2* **1996**, *8*, 1527–1528.
[52] W. E. Bennett, D. E. Broberg, N. C. Baenziger, *Inorg. Chem.* **1973**, *12*, 930–936.
[53] J. Janczak, R. Kubiak, *J. Alloys Compd.* **1994**, *204*, 5–11.
[54] R. Kubiak, J. Janczak, *J. Alloys Compd.* **1992**, *189*, 107–111.
[55] CASTEP: Cambridge Serial Total Energy Package, *Ab initio Molecular Dynamics Program with Conjugate Gradient Minimisation (CG) for the Electronic Energy*, Version 4.6, Release 1, June **2001**, Accelrys Inc., CASTEP Users Guide, San Diego: Accelrys Inc., **2001**; V. Milman, B. Winkler, J. A. White, C. J. Pickard, M. C. Payne, E. V. Akhmatskaya, R. H. Nobes, *Int. J. Quantum Chem.* **2000**, *77*, 895–910; J. P. Perdew, *Phys. Rev. B* **1986**, *33*, 8822–8824; A. D. Becke, *Phys. Rev. A* **1988**, *38*, 3098–3100; J. P. Perdew, J. A. Chevary, S. H. Vosko, K. A. Jackson, D. J. Singh, C. Fiolhais, *Phys. Rev. B* **1992**, *46*, 6671–6687.
[56] a) C. G. Claessens, A. Gouloumis, M. Barthel, Y. Chen, G. Martin, F. Argulló-López, I. Ledoux-Rak, J. Zyss, M. Hanack, *J. Porphyrins Phthalocyanines* **2003**, *7*, 291–295; b) M. Barthel, D. Dini, S. Vagin, M. Hanack, *Eur. J. Org. Chem.* **2002**, 3756–3762; c) M. Bartherl, M. Hanack, *J. Porphyrins Phthalocyanines* **2000**, *4*, 635–638.
[57] ASTM G59–97, "Test method for conducting potentiodynamic polarization resistance measurements", *Annual book of ASTM*, Vol. 3.02, Philadelphia, PA, **1997**.
[58] ASTM G102–89, "Standard practice for calculation of corrosion rates and related information from electrochemical measurements", *Annual book of ASTM*, *Vol. 3.02*, Philadelphia, PA, **1989**.
[59] J. N. Al-Hajji, M. R. Reda, *Corrosion* **1993**, 49, 363–371.
[60] Bruker Analytical X-ray Systems, SMART: Bruker Molecular Analysis Research Tool, Version 5.618, **2000**.
[61] Bruker Analytical X-ray Systems, SAINT + NT Version 6.04, **2001**.
[62] Bruker Analytical X-ray Systems, SHELXTL-NT Version 6.10, **2000**.
[63] G. M. Sheldrick, SHELX-97, Program for Crystal Structure Solution, University of Göttingen (Germany) **1993**.
[64] L. J. Farrugia, *J. Appl. Crystallogr.* **1999**, *32*, 837–838. Win GX Program set.
[65] M. Nardelli, *J. Appl. Crystallogr.* **1995**, *28*, 659—660, PARST program, released Nov. **1999**.
[66] L. J. Farrugia, *J. Appl. Crystallogr.* **1997**, *30*, 565–566, ORTEP 3 Program.
[67] Mercury 1.1.2, Copyright CCDC **2001–2002**, All rights reserved. For more information about this application, please contact User Sup-

port by e-mail at: support@ccdc.cam.ac.uk, or at the www site http://www.ccdc.cam.ac.uk/mercury/.
[68] ASM handbook, *Corrosion*, Vol. *13*, pp. 1232, ninth edition, **1987**.
[69] *General Purpose Electrochemical Software* (GPES) v. 4.4. (Provided with Autolab PGSTAT-3, Eco Chemie B. V., Utrecht, The Netherlands) with PC software control.
[70] G. E. Stansbury, R. A. Buchanan, *Fundamentals of electrochemical corrosion*, Chap. 6, pp. 233, ASM international, **2000**.

Received: September 17, 2004
Published online: February 25, 2005

